THE JOURNAL OF PHYSICAL CHEMISTRY Letters

pubs.acs.org/JPCL Letter

Extracting Electronic Transition Bands of Adsorbates from Molecule−Plasmon Excitation Coupling

Tefera E. Tesema, Hamed Kookhaee, and Terefe G. Habteyes*

Cite This: J. Phys. Chem. Lett. 2020, 11, 3507−3514 Read Online

ACCESS | Metrics & More | Article Recommendations | Supporting Information

ABSTRACT: The coupling between molecular electronic and particle plasmon excitations can result in various intriguing outcomes depending on how strongly or weakly the excitations couple to compete with their respective decay rates. In this work, using methylene blue and thionine dyes as model systems, we show that the electronic absorption band of resonant adsorbates can be determined with submonolayer sensitivity from the weak molecule−plasmon excitation coupling that results in the attenuation on the plasmonic absorption band. The extracted spectra are strongly similar to the absorption spectra of the corresponding molecules in solution, apart from the expected spectral red-shift and broadening. Interestingly, the adsorption isotherms determined on the basis of the magnitude of the attenuation correlate linearly with that determined from the adsorbate-induced plasmon resonance red-shift. The results demonstrate that in the weak coupling regimes the plasmon modes can be considered as an environment that supplies energy to and takes energy from the adsorbates.

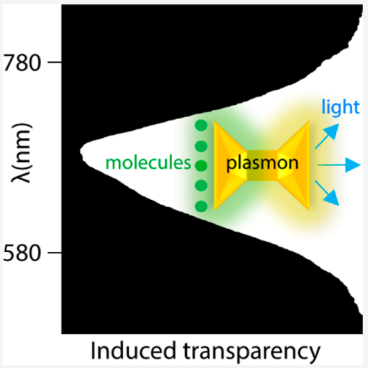

The interaction between molecular electronic and particle plasmon resonances is a rich physical process that enables detection of a single molecule[1,2] and creation of entangled states for quantum information processing.[3] In the weak coupling regime, the molecular excitation and emission processes can be modified by the high mode density of the surface plasmon, which can result in surface-enhanced spectroscopy.[1,4−7] In the strong coupling regime, entangled states that can be used as a quantum information system can be generated.[8,9] The strong and weak coupling regimes can be distinguished on the basis of atom-field interaction theory using a coupling constant (g) defined by the equation $g = \mu[\omega_0/(2\hbar\varepsilon_0 V)]^{1/2}$, where $\hbar$ is the reduced Planck's constant, ε_0 the vacuum permittivity constant, ω_0 the transition frequency of the molecule, μ the dipole matrix element of the atomic or molecular transition, and V the effective cavity volume.[10] To realize the strong coupling regime, g has to be large enough to overcome the resonant and nonresonant losses of the cavity.[10] The strength of the coupling scales with the number of atoms or molecules (N) in the cavity as $\sqrt{N}g$.[10] Practically, strong coupling has been observed at room temperature when a thick layer of J-aggregates is excited in the proximity of the plasmonic surfaces.[11−21] There is only one report that claims the observation of strong coupling for <10 molecules at room temperature.[9] In this experiment, spectral splitting has been observed when methylene blue (MB) molecules are aligned vertically along the electric field in a particle−film plasmonic system that provides an extremely small cavity volume. No spectral splitting has been observed when the MB molecules adsorb to the gold surface randomly. In general, observation of strong coupling requires significant experimental perfection to achieve a large coupling constant by fabricating a cavity with a high quality factor and with the resonance tuned to the electronic transition energy of the emitter.[8,10,22,23]

Despite the stringent requirements needed for strong coupling, the observation of spectral asymmetry in plasmonic systems coupled to molecular aggregates in a random geometry can be confused with strong coupling. For example, the broad absorption spectra of silver islands are split into two peaks upon adsorption of rhodamine B, while only one peak is observed in the fluorescence excitation spectra.[24] On the contrary, a recent experimental demonstration indicates that splitting in photoluminescence spectra is more reliable evidence of strong coupling than the splitting in the dark-field scattering spectra.[12] In the weak coupling regimes, the surface plasmon may be treated as an environment that supplies and absorbs energy to and from the molecule depending on the molecule−surface proximity, spectral overlap, and orientation of the dipole with respect to the surface field.[25,26] The plasmon surface field enhances the excitation of the molecule, and the molecular excitation can efficiently couple back to the plasmon modes that can lead to plasmon-coupled photon emission.[27−29] This interaction can lead to the appearance of spectral splitting in the absorption

Received: March 5, 2020
Accepted: April 17, 2020
Published: April 17, 2020

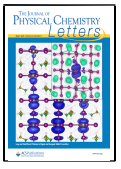

https://dx.doi.org/10.1021/acs.jpclett.0c00734
J. Phys. Chem. Lett. 2020, 11, 3507−3514

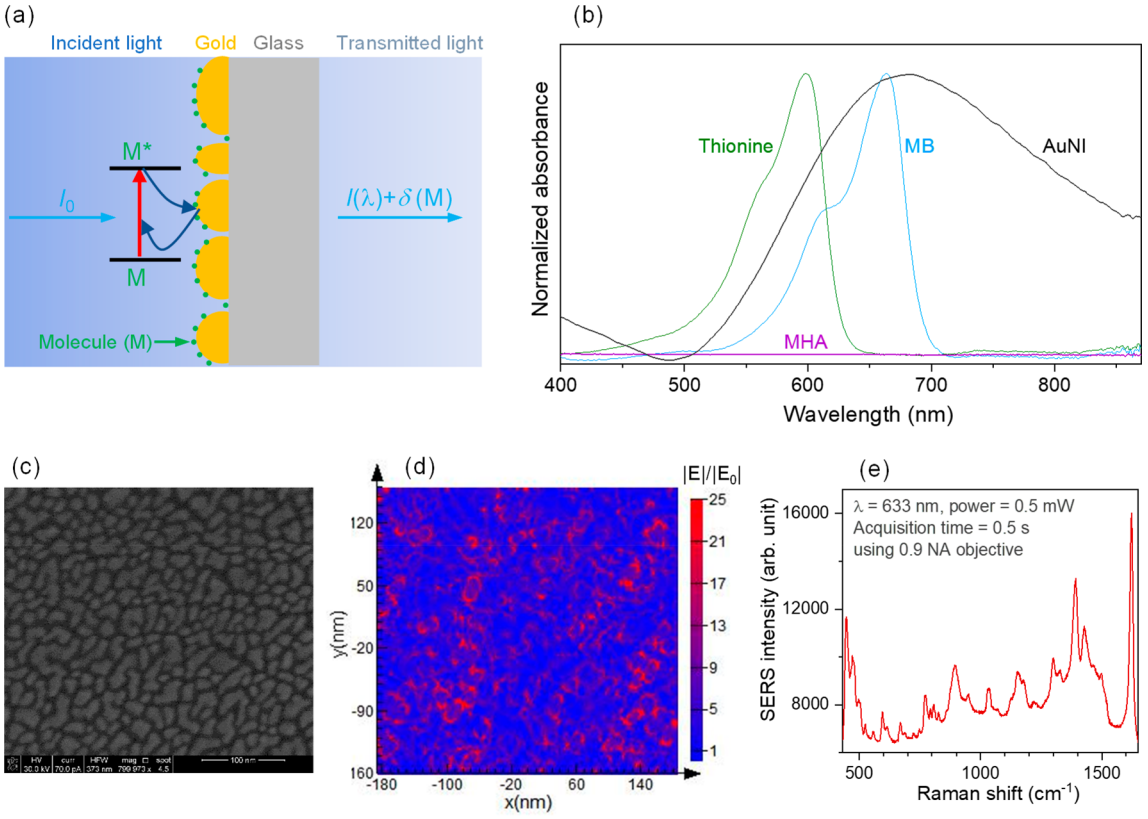

Figure 1. Principle of excitation coupling between molecule and particle resonances. (a) Schematic showing the processes in the excitation and transmission measurement. The molecules, represented by the green dots, are adsorbed on the gold nanostructures that are supported on glass. The incident light with intensity I_0 excites both the electronic transition of the molecule (M → M* transition) and the plasmon resonance of the gold nanostructures. The plasmon resonance enhances the rate of molecular excitation, and the excitation energy of the molecule couples back to the surface plasmon, modifying the intensity of the transmitted light. (b) Absorption spectra of AuNIs, MB, thionine, and MHA as labeled. (c) Scanning electron microscope image of the AuNIs formed by electron-beam evaporation of gold on glass. (d) Calculated electric-field distribution at the Au−glass interface at a λ of 680 nm. (e) Surface-enhanced Raman spectroscopy of MB adsorbed on the AuNIs confirms the field enhancement.

and scattering spectra, although no new mixed states may be created. In principle, it should be possible to extract the absorption/emission band of molecular adsorbates from the plasmonic environment through careful analysis of plasmon−molecule excitation coupling. We note that the electronic transition energy of adsorbates is critical for understanding surface chemical, electronic, and optical properties. For example, determining the spectral overlap of the excitation wavelength with the molecular electronic and particle plasmon resonances should be the first step in explaining the mechanisms of surface-enhanced Raman scattering[30,31] and plasmon-driven photochemistry.[32]

In this work, the hypothesis of determining the adsorbate absorption band from molecule−plasmon excitation coupling is tested by analyzing the absorption spectra of plasmonic gold nanoislands (AuNIs) with MB and thionine adsorbates. We note that for π-conjugated molecules with a fused aromatic ring that includes our model systems, the molecules are oriented parallel to the surface due to a π-stacking type of surface−molecule interaction, resulting in the molecular dipole orientation mainly parallel to the surface.[33,34] For this adsorption geometry, strong coupling can be ruled out. However, because of rough surfaces, the less than perfect planar orientation of the molecules on the surface, and the availability of different plasmon modes,[33,35] the surface−molecule energy transfer can be efficient to completely quench the fluorescence of the adsorbates.[36] In fact, fluorescence background quenching by metal surfaces is one of the reasons for the success of surface-enhanced Raman spectroscopy.[35] Owing to the surface−molecule energy transfer and the subsequent plasmon-coupled photon emission that can lead to enhanced transmission, we observe attenuation in the absorption spectra of the AuNI at the absorption wavelengths of the adsorbed dye molecules. The absorption bands of the adsorbates are extracted from the changes induced on the absorption spectra of the plasmon resonances through systematic experimental and data analysis procedures.

The schematic in Figure 1a shows the principle of the experiment for extracting the perturbation $\delta(M)$ on the optical transmission of the plasmonic system induced by the coupling of the molecular electronic excitation. The incident light with intensity I_0 excites both the electronic transition of the molecule and the plasmon resonance of the AuNIs. The absorption spectra in Figure 1b indicate the overlap between the electronic transitions of the molecules (MB and thionine) and the broad plasmon resonance of the AuNIs (Figure 1c) that have a thickness of ∼5 nm as determined using an atomic force microscope (see Figure S1). It is well-known that evaporation of metals at this thickness creates island structures that support localized surface plasmon resonances.[37] The electric field at the metal−glass interface calculated using the finite-difference time-domain method of electromagnetic

https://dx.doi.org/10.1021/acs.jpclett.0c00734
J. Phys. Chem. Lett. 2020, 11, 3507−3514

simulation indicates the plasmon near-field enhancement around the AuNIs (Figure 1d). The surface-enhanced Raman scattering signal of submonolayer MB adsorbed on the AuNIs (Figure 1e) confirms the field enhancement. The enhanced surface field pumps the electronic excitation of the adsorbates, and the excitation energy of the molecule couples back to the surface plasmon, modifying the transmitted light intensity as $I(\lambda) + \delta(M)$, where I is the wavelength (λ)-dependent intensity of the transmitted light assuming that the effect of the adsorbate is limited to shifting the plasmon resonance wavelength. For AuNIs with nonresonant adsorbates for which $\delta(M) = 0$, the absorbance A_N can be expressed using Beers law as

$$A_N = -\log\left[\frac{I(\lambda)}{I_0}\right] \quad (1)$$

Similarly, for the AuNIs with resonant adsorbates that induce a plasmon resonance wavelength shift similar to that of the nonresonant one, the absorbance A_R can be written as

$$A_R = -\log\left[\frac{I(\lambda) + \delta(M)}{I_0}\right] \quad (2)$$

Assuming that the coupling is weak such that the symmetry of the resonances is not affected by Fano-type interference effects,[38,39] the change in the absorbance (ΔA) due to molecule−plasmon excitation coupling of the resonant adsorbates can then be calculated using the nonresonant adsorbate as a reference.

$$\Delta A = A_R - A_N = \log\left[1 + \frac{\delta(M)}{I(\lambda)}\right] \quad (3)$$

where $\delta(M) < 0$ when the plasmonic absorbance is attenuated due to the coupling of the molecular excitation energy to the surface plasmon mode that results in enhanced transmission at the absorption wavelength of the adsorbate. On the other hand, $\delta(M) > 0$ when the adsorbate has an additive effect on the absorption. It is important to note that $\delta(M)$ is extremely small compared to the large extinction cross section of the plasmonic metal nanostructures. Consequently, determining the absorption band of the adsorbate on the basis of eq 3 requires measurement of the plasmon resonance of the same metal nanostructures before and after adsorption of the analyte molecules.

The principle described above is implemented by depositing the AuNIs on one of the outer surfaces of quartz cuvettes so that the rigid cuvette mount of the absorption spectrophotometer (see Methods for sample fabrication, preparation, and measurement details) ensures probing of the same plasmonic surfaces before and after adsorption of the analyte molecules. In Figure 2a, the absorption spectra of the bare AuNIs (AuNI-1 and AuNI-2) are shown by the dotted black and red lines. The absorption spectra of the same AuNIs after adsorption of nonresonant 6-mercaptohexanoic acid (MHA) and resonant MB molecules are shown by the solid black and red lines, respectively, as labeled in Figure 2a. The adsorption of both MHA and MB has resulted in significant and comparable red-shifting of the respective plasmon resonances. More importantly, the adsorption of MB has induced an attenuation (elbowing) effect as can be seen by comparing the solid red line (A_R) to the solid black line (A_N) in Figure 2a. The elbowing effect appears to take place at the absorption

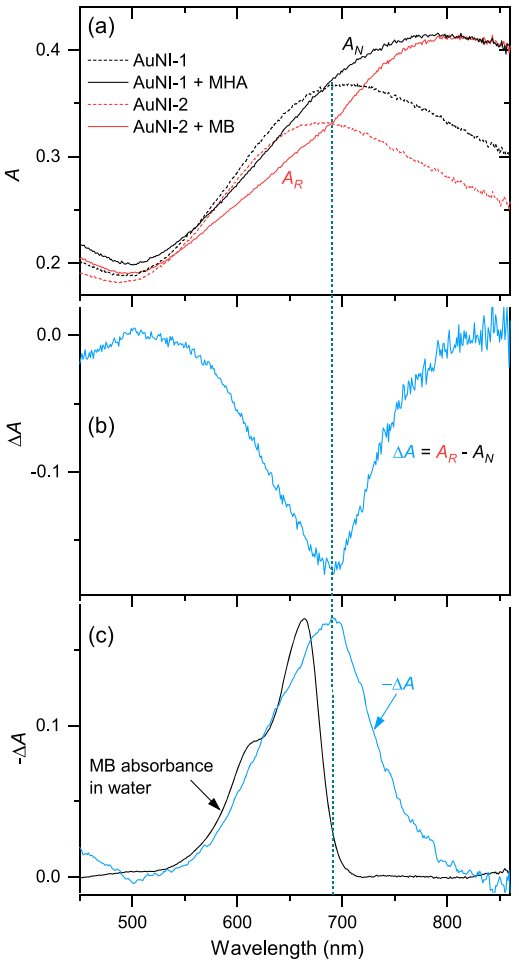

Figure 2. Experimental demonstration of the principle for determining the adsorbate absorption band from induced absorbance attenuation of the localized surface plasmon resonance. (a) The dotted black and red lines are absorption spectra of two different plasmonic AuNIs (labeled as AuNI-1 and AuNI-2) before adsorption of the analyte molecules. The solid lines labeled A_N and A_R show the absorption spectra after the nonresonant MHA and resonant MB molecules are adsorbed on AuNI-1 and AuNI-2, respectively. (b) Difference spectrum obtained by subtracting A_N from A_R. (c) Inverted difference spectrum after adjacent averaging (blue) compared to the normalized absorption spectrum of MB in water (black).

wavelength of the adsorbate and is in agreement with the observation of wavelength-dependent attenuation of surface plasmon resonance reflectivity reported for a 40 nm thick silver film with a zinc phthalocyanine-tetrasulfonic acid adsorbate.[40] Hence, the attenuation effect in the presence of MB is attributed to enhanced transmission due to the coupling of the molecular excitation energy to the plasmon resonance.

The magnitude and shape of the absorbance reduction are obtained by subtracting A_N from A_R (according to eq 3) after normalizing the two curves such that they have the same minima and maxima, and the result (ΔA) is plotted in Figure 2b. Clearly, a window of transparency that closely matches the absorption band of the MB adsorbate is observed. The inverted spectrum ($-\Delta A$) is reasonably similar to the normalized absorption spectrum of MB in water as shown in Figure 2c. We note that in Figure 2a, the peak position of the A_N spectrum does not perfectly match that of the A_R. To confirm the effect of the relative peak position of the reference spectra on the

https://dx.doi.org/10.1021/acs.jpclett.0c00734
J. Phys. Chem. Lett. 2020, 11, 3507−3514

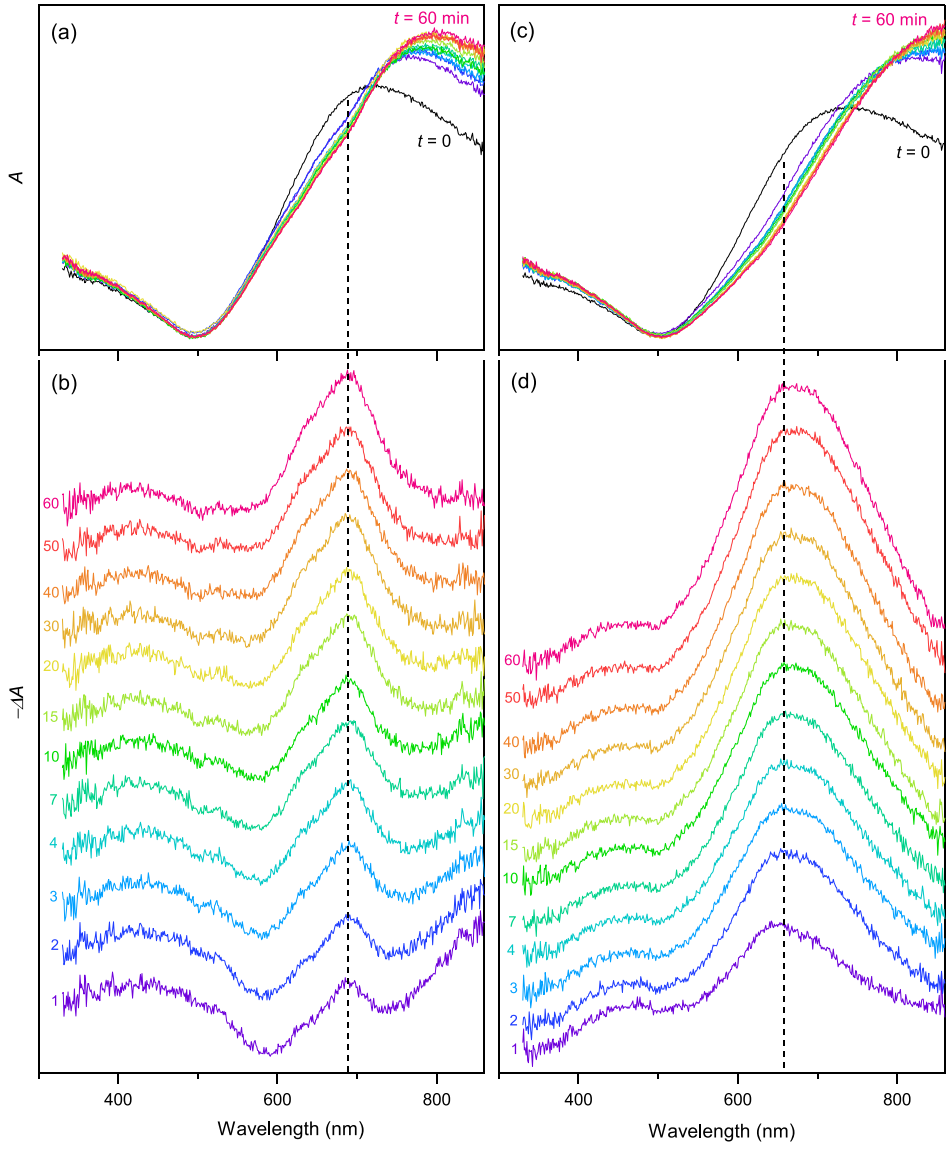

Figure 3. Dependence of absorbance attenuation on adsorption time. (a) Absorption spectra of the same AuNIs as the adsorption time of MB is increased from 0 min (black line, bare AuNIs) to 60 min (pink line). (b) Difference spectra obtained by subtracting the spectrum of AuNI-MHA from the AuNI-MB spectra at different adsorption times. The numbers next to each plot are the adsorption time in minutes. (c and d) Same as panels a and b, respectively, for the thionine adsorbate.

peak position of the ΔA spectra, the adsorption time of MHA has been varied such that the A_N peak position is swept from the blue side to the red side of the A_R peak position as shown in Figure S2a. It is found that the peak position of ΔA remains the same when the AuNI−MHA spectra with different peak positions are used as references (see Figure S2b). This is because the slope of the A_N lines is approximately constant in the region where attenuation is observed in the A_N spectra. As a result, the same reference spectrum is used in the rest of our analysis.

As one can see in Figure 2c, with respect to the solution phase absorption band, the inverted spectrum is broadened and is shifted to the red by ∼24 nm, which is in agreement with the results reported by Darby et al. using integrating sphere absorption spectroscopy of Rhodamine 700 adsorbed on silver nanoparticles.[41] We note that enhanced transmission at the absorption band of >30 nm thick cyanine J-aggregates has been observed when the aggregates are supported on arrays of 200 nm thick gold and silver nanoholes with 100 nm in diameter,[42,43] while our observation is for the submonolayer of adsorbates as demonstrated next.

In all of our experiments, the adsorption of the analyte molecules is carried out by immersing the AuNIs in 10−220 μM solutions for 1−2 h. For concentrations of <10 μM, adsorption was not effective (see Figure S3). It has been reported that in this concentration range, adsorption of MB on gold results in submonolayer to monolayer surface coverage even when the gold surface is prefunctionalized to enhance the adsorption.[44] This is not surprising considering that the surface−molecule interaction is governed by van der Waals dispersion forces.[34] In our experiment, the adsorption properties are studied by measuring the absorption spectra of the same AuNIs after every successive increase in the adsorption times starting with a 1 min duration. The results presented in Figure 3a show that as the adsorption time increases, the plasmonic absorbance at the absorption

https://dx.doi.org/10.1021/acs.jpclett.0c00734
J. Phys. Chem. Lett. 2020, 11, 3507−3514

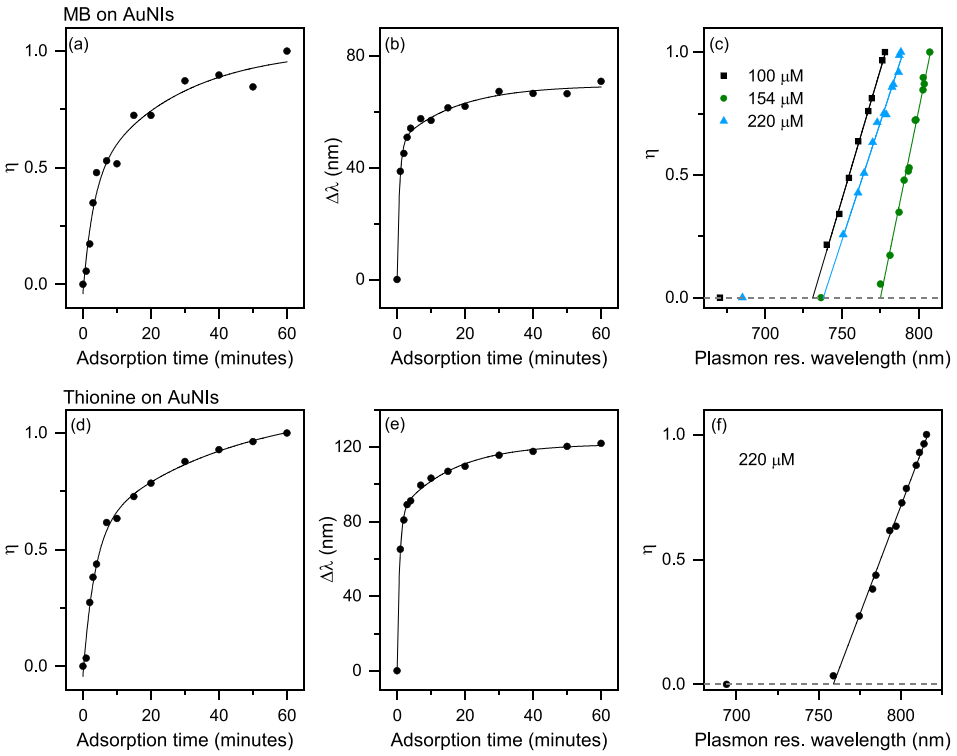

Figure 4. Adsorption isotherms and correlation. (a and d) Adsorption isotherms determined from absorbance changes induced by MB and thionine adsorbates, respectively, on AuNIs. (b and e) Adsorption isotherms determined from the plasmon resonance wavelength shifts induced by MB and thionine adsorbates, respectively. (c and f) Correlation between normalized absorbance changes and plasmon resonance wavelength shift for MB and thionine adsorbates, respectively. The three correlation plots in panel c indicate that the linear trend is reproducible at different concentrations of the solution in which the substrate is immersed for adsorbing the molecules.

wavelength of the MB adsorbate decreases continuously. The effect of the adsorption time is more apparent in the difference spectra plotted in Figure 3b. The signature of the adsorbate absorption band that results from molecule−plasmon excitation coupling is observed even after adsorption for 1 min. As one can see in Figure 3b, the magnitude of ΔA increases with an increase in adsorption time as the number of MB adsorbates per unit area increases. Interestingly, the shoulder peak that is observed in the solution phase absorption spectrum of MB (Figure 1b) is reproduced in the series of spectra in Figure 3b (see also Figure S4 for a more quantitative comparison).

The similarity of the adsorbate and solution phase absorption spectra indicates that the inherent electronic band of the molecule is not altered by the possible optical interference between the molecular and plasmon resonances. We note that it is easier to discern spectral asymmetry induced by Fano-type interference effects when the original spectra have Lorentzian line shapes.[38] To quantify the significance of optical interference effects, we compare the dark-field scattering spectra of gold nanorods (AuNRs) without and with MB adsorbates as shown in Figure S5. As one can see by comparing the results in panels a and b of Figure S5, adsorption of MB on the AuNRs has resulted in spectral broadening, red-shifting, and a decrease in the intensity on the single-particle plasmon resonance scattering spectra, which can be attributed to the damping effect due to the plasmon-pumped adsorbate excitation as in the well-known chemical interface plasmon damping effect.[45−47] However, the scattering spectra of the AuNRs with the MB adsorbate fit to a Lorentzian function with an R^2 value of >0.99 (see Figure S5c), indicating the absence of spectral asymmetry due to interference effects. Therefore, the similarity of the adsorbate spectra to that of the solution phase suggests a coupling regime in which molecule−plasmon energy exchange takes place, while the optical interference effect between the resonances is negligible. It is also important to note that the observation of the elbowing effect at the absorption wavelength of the adsorbate is indicative of the richness of the plasmon modes in the evaporated metal film that is not possible in quasi-crystalline single particles that have plasmon resonances dominated by a particular mode.

In the absence of optical interference effects that alter the inherent resonance line shapes, we can assume that the adsorbate spectral properties are governed mainly by the surface−molecule chemical interaction. To obtain insight into the adsorption properties depending on the molecular structures, the results obtained for the MB adsorbate (Figure 3a,b) are compared to that of thionine (Figure 3c,d). The difference spectra in Figure 3d indicate that the absorption band for the thionine adsorbate has shifted to the red by >50 nm with respect to the absorption band of thionine in water that peaks at 599 nm (see Figure 1b), compared to the 24 nm red-shift for MB. This large wavelength shift for the thionine adsorbate is accompanied by drastic line width broadening. The larger wavelength shift and broadening for thionine than for MB can be attributed to the replacement of the relatively bulky methyl groups at the N-terminus with hydrogen atoms that favors stronger thionine−surface interaction through the amine functional groups because there is less steric hindrance

https://dx.doi.org/10.1021/acs.jpclett.0c00734
J. Phys. Chem. Lett. 2020, 11, 3507−3514

as the adsorption geometry reported by Guo et al. suggests.[34] The stronger surface−molecule interaction for thionine than for MB can be the thermodynamic driving force for the plasmon-driven N-demethylation of MB.[32,36,48]

The absorbance changes observed as a function of adsorption time are analyzed on the basis of adsorption isotherms obtained using the integral area under the curves in panels b and d of Figure 3. To facilitate the analysis, we define an adsorption parameter as $\eta = I_t/I_m$, where I_t and I_m are the integral areas at any time (t) and infinite time when a monolayer (m) surface coverage is assumed, respectively. As shown in panels a and d of Figure 4 for MB and thionine adsorbates, respectively, η increases with time first rapidly and then plateaus, indicating the saturation of surface coverage. The adsorption isotherms determined from the magnitude of absorbance attenuation compare favorably with the isotherms determined from the plasmon resonance wavelength shift (Figure 4b,e), which is a well-established procedure for quantifying adsorption properties.[49] However, it is important to note that the plasmon wavelength shift ($\Delta\lambda$) increases much faster than η initially. Fitting a biexponential function ($\Delta\lambda = \Delta\lambda_m - ae^{-t/\tau_1} - be^{-t/\tau_2}$, where $\Delta\lambda_m$ is the plasmon resonance wavelength shift at a monolayer surface coverage) to the specific data presented in panels b and e of Figure 4 produces the following values: $\Delta\lambda_m$ = 69 nm, τ_1 = 0.74 min, and τ_2 = 17 min for MB, and $\Delta\lambda_m$ = 122 nm, τ_1 = 0.76 min, and τ_2 = 16 min for thionine. The time constants for MB and thionine adsorbates appear comparable possibly due to the lack of data points for adsorption times of <1 min. The wavelength shift varies significantly from sample to sample, ranging from 69 to 113 nm for MB on five different AuNIs within 1 h of adsorption time, while adsorption of thionine on most AuNIs shifts the resonance wavelength outside the detection window of our spectrometer as shown in Figure 3c. It is interesting to note that the larger plasmon resonance shift for thionine corresponds to the more pronounced molecular resonance shift as mentioned earlier in comparing the results in panels b and d of Figure 3, confirming the stronger surface−molecule interaction of thionine. Overall, the resonance wavelength shift observed in our experiment is larger than the maximum shift (55 nm) observed during the adsorption of rhodamine 6G on silver nanostructures.[50] However, it is important to note that the extent of the shift increases significantly with an increase in the resonance wavelength.[50] Hence, the plasmon shift around the MB resonance (~688 nm) is expected to be significantly larger than the shift around the rhodamine 6G resonance (~560 nm). In addition, in our experiment, the AuNIs are used as evaporated, and the rough structure and large surface area can result in a large number of adsorbates per unit volume of metal.

In panels c and f of Figure 4, η is plotted as a function of the plasmon resonance peak wavelength. Interestingly, a linear correlation is obtained excluding the data point for the bare AuNIs as shown by the plots. The deviation of the data point for the bare AuNIs from the linear trend can be attributed to the lack of a clear background reference for extracting the adsorbate-induced change in the absorbance, while the plasmon resonance shift can be monitored accurately and unambiguously. A more accurate procedure for extracting η is particularly important at very short incubation times that results in a low number density of adsorbates. We note that the magnitude of ΔA depends on the relative peak position of the reference spectra, although its peak position remains constant as illustrated in Figure S2b.

So far, the reduction of the plasmonic absorbance at the absorption band of the adsorbates has mainly been discussed in terms of the molecular electronic excitation energy coupling to the surface plasmon modes. However, it is important to note that the plasmon surface field also pumps the excitation of the adsorbates as illustrated by the schematics in Figure 1a. The plasmon−molecule interaction at the excitation step may be considered as a plasmon damping process in which the surface plasmon is dephasing through plasmon-pumped adsorbate excitation.[24,45] The excited adsorbates (emitters) can be considered as dipole sources that can excite plasmon modes. It has been theoretically predicted that dipole sources can excite plasmon modes that remain dark under incident plane wave source illumination.[51−53] Because the adsorbates are directly adsorbed on the metal surface, vibrational relation in the excited electronic state may be unlikely to compete with the excitation coupling to the plasmon mode. This may explain the similarity of the ΔA spectral shape particularly for MB (Figure 3b) to the corresponding absorption band in solution as opposed to the fluorescence band, which appears as the mirror image of the former.

In summary, this work demonstrates that the electronic absorption band of molecular adsorbates on plasmonic surfaces can be determined on the basis of molecule−plasmon excitation coupling that attenuates the absorbance of the plasmonic metal nanostructures. The systematic analysis of the experimental results shows that in the weak coupling regimes the plasmon surface modes can be treated as an environment to which molecular excitations scatter, and in turn, the electronic absorption band of the adsorbates can be extracted from the environment. This procedure provides submonolayer sensitivity to determine the adsorbate electronic transition band, which is difficult to quantify using conventional approaches. The extracted spectra indicate that the absorption bands are broadened and red-shifted with respect to solution phase spectra due to surface−molecule interaction.

METHODS

Preparation of Gold Nanoislands (AuNIs). The AuNIs with different thicknesses are formed naturally during the electron-beam evaporation of gold on one side of the outer of a quartz cuvette at a rate of 0.2 Å/s at a chamber pressure of $1-2 \times 10^{-6}$ Torr. For structural analysis, the metals are also deposited on an oxide-coated silicon wafer during the same evaporation process. The thickness and the deposition rate of films were monitored by using a quartz crystal microbalance. After the analysis of the optical responses of different thicknesses, the AuNIs with ~5 nm are chosen for further studies of molecule−plasmon excitation coupling.

Adsorption of Molecules on AuNIs. The analyte molecules (methylene blue, thionine, and 6-mercaptohexanoic acid) are adsorbed on the AuNIs by immersing the metal-coated cuvette side into the solution for different durations ranging from 1 to 60 min. Methylene blue and thionine are dissolved in water, while 6-mercaptohexanoic acid is dissolved in ethanol, with concentrations ranging from 1 to 220 μM. The adsorption on the AuNIs is carried out by carefully moving the gold-coated side of the quartz cuvette vertically with the aid of a mechanical stage until only the gold-coated side of the cuvette is sufficiently immersed in the solution. Then the system is covered with aluminum foil and incubated for a specified

https://dx.doi.org/10.1021/acs.jpclett.0c00734
J. Phys. Chem. Lett. 2020, 11, 3507−3514

period of time at room temperature. At the end of the incubation, the film is rinsed gently with ultrapure water and dried in air.

Absorbance Measurement. The absorption spectra of the AuNIs have been recorded with a Shimadzu UV-2450 ultraviolet−visible spectrophotometer using air as a baseline. That is, the quartz cuvette with the AuNI is placed in the sample cell, while the reference cell is empty. First, the absorption spectra of the cuvette with the bare AuNIs are recorded. Then, the measurement is repeated on the same AuNIs after the analyte molecules are adsorbed. In addition to the fact that the measurement before and after adsorption must be carried out on the same AuNIs, it is important that the spectrometer remain on during the adsorption process so that the adsorption effect is not obscured by the fluctuation of the incident light intensity.

Structural Characterization. The structure of the fabricated gold nanoislands is characterized using the scanning electron microscope (Quanta 3D FEG) to imagine the lateral distribution and the atomic force microscope (Neaspec GmbH) to determine the height.

Electromagnetic Simulation. The near-field distribution in Figure 1d is calculated using the finite-difference time-domain method of electromagnetic simulation using the Lumerical software. Two sources with orthogonal polarization in the sample plane are introduced into the simulation region using a total-field scattered-field source. The structure of the AuNIs is defined by importing the scanning electron microscope (SEM) image, and its accuracy in mimicking the actual structures is limited by the spatial resolution of the SEM. The gold structure is placed on a SiO_2 substrate. Gold is modeled using the dielectric function data of Johnson and Christy, and SiO_2 is modeled using the Palik data. A grid size of 0.5 nm is used in all three directions in the region where the source is introduced.

■ ASSOCIATED CONTENT

Supporting Information

The Supporting Information is available free of charge at https://pubs.acs.org/doi/10.1021/acs.jpclett.0c00734.

Supporting figures (PDF)

■ AUTHOR INFORMATION

Corresponding Author

Terefe G. Habteyes − *Department of Chemistry and Chemical Biology and Center for High Technology Materials, University of New Mexico, Albuquerque, New Mexico 87131, United States*; orcid.org/0000-0001-5978-6464; Email: habteyes@unm.edu

Authors

Tefera E. Tesema − *Department of Chemistry and Chemical Biology and Center for High Technology Materials, University of New Mexico, Albuquerque, New Mexico 87131, United States*

Hamed Kookhaee − *Department of Chemistry and Chemical Biology and Center for High Technology Materials, University of New Mexico, Albuquerque, New Mexico 87131, United States*

Complete contact information is available at: https://pubs.acs.org/10.1021/acs.jpclett.0c00734

Notes

The authors declare no competing financial interest.

■ ACKNOWLEDGMENTS

This research has been supported by U.S. Air Force Office of Scientific Research Grant FA9550-18-1-0512 and U.S. National Science Foundation Grant 1651478. Evaporation of gold was performed at the Center for Integrated Nanotechnologies (CINT), an Office of Science User Facility operated for the U.S. Department of Energy (DOE) Office of Science by Los Alamos National Laboratory (Contract DE-AC52-06NA25396) and Sandia National Laboratories (Contract DE-NA-0003525).

■ REFERENCES

(1) Kinkhabwala, A.; Yu, Z. F.; Fan, S. H.; Avlasevich, Y.; Mullen, K.; Moerner, W. E. Large Single-Molecule Fluorescence Enhancements Produced by a Bowtie Nanoantenna. *Nat. Photonics* **2009**, *3*, 654−657.

(2) Taylor, A. B.; Zijlstra, P. Single-Molecule Plasmon Sensing: Current Status and Future Prospects. *ACS Sensors* **2017**, *2*, 1103−1122.

(3) Baranov, D. G.; Wersall, M.; Cuadra, J.; Antosiewicz, T. J.; Shegai, T. Novel Nanostructures and Materials for Strong Light Matter Interactions. *ACS Photonics* **2018**, *5*, 24−42.

(4) Zrimsek, A. B.; Chiang, N. H.; Mattei, M.; Zaleski, S.; McAnally, M. O.; Chapman, C. T.; Henry, A. I.; Schatz, G. C.; Van Duyne, R. P. Single-Molecule Chemistry with Surface- and Tip-Enhanced Raman Spectroscopy. *Chem. Rev.* **2017**, *117*, 7583−7613.

(5) Sun, G.; Khurgin, J. B.; Soref, R. A. Practical Enhancement of Photoluminescence by Metal Nanoparticles. *Appl. Phys. Lett.* **2009**, *94*, 101103.

(6) Itoh, T.; Yamamoto, Y. S.; Ozaki, Y. Plasmon-Enhanced Spectroscopy of Absorption and Spontaneous Emissions Explained Using Cavity Quantum Optics. *Chem. Soc. Rev.* **2017**, *46*, 3904−3921.

(7) Wang, C.-F.; Addamane, S.; Patra, B.; Lebron, C. R.; Haq, S.; Balakrishnan, G.; Malloy, K. J.; Habteyes, T. G. Revealing Temperature-Dependent Absorption and Emission Enhancement Factors in Plasmon Coupled Semiconductor Heterostructures. *ACS Appl. El. Mater.* **2019**, *1*, 1439−1448.

(8) Torma, P.; Barnes, W. L. Strong Coupling between Surface Plasmon Polaritons and Emitters: A Review. *Rep. Prog. Phys.* **2015**, *78*, 013901.

(9) Chikkaraddy, R.; de Nijs, B.; Benz, F.; Barrow, S. J.; Scherman, O. A.; Rosta, E.; Demetriadou, A.; Fox, P.; Hess, O.; Baumberg, J. J. Single-Molecule Strong Coupling at Room Temperature in Plasmonic Nanocavities. *Nature* **2016**, *535*, 127−130.

(10) Fox, M. *Quantum Optics: An Introduction*; Oxford University Press: Oxford, U.K., 2006.

(11) Balci, S.; Kucukoz, B.; Balci, O.; Karatay, A.; Kocabas, C.; Yaglioglu, G. Tunable Plexcitonic Nanoparticles: A Model System for Studying Plasmon-Exciton Interaction from the Weak to the Ultrastrong Coupling Regime. *ACS Photonics* **2016**, *3*, 2010−2016.

(12) Wersall, M.; Cuadra, J.; Antosiewicz, T. J.; Balci, S.; Shegai, T. Observation of Mode Splitting in Photoluminescence of Individual Plasmonic Nanoparticles Strongly Coupled to Molecular Excitons. *Nano Lett.* **2017**, *17*, 551−558.

(13) Zengin, G.; Wersall, M.; Nilsson, S.; Antosiewicz, T. J.; Kall, M.; Shegai, T. Realizing Strong Light-Matter Interactions between Single-Nanoparticle Plasmons and Molecular Excitons at Ambient Conditions. *Phys. Rev. Lett.* **2015**, *114*, 157401.

(14) DeLacy, B. G.; Miller, O. D.; Hsu, C. W.; Zander, Z.; Lacey, S.; Yagloski, R.; Fountain, A. W.; Valdes, E.; Anquillare, E.; Soljacic, M.; Johnson, S. G.; Joannopoulos, J. D. Coherent Plasmon-Exciton Coupling in Silver Platelet-J-Aggregate Nanocomposites. *Nano Lett.* **2015**, *15*, 2588−2593.

(15) Vasa, P.; Wang, W.; Pomraenke, R.; Lammers, M.; Maiuri, M.; Manzoni, C.; Cerullo, G.; Lienau, C. Real-Time Observation of Ultrafast Rabi Oscillations between Excitons and Plasmons in Metal Nanostructures with J-Aggregates. *Nat. Photonics* **2013**, *7*, 128−132.
(16) Schlather, A. E.; Large, N.; Urban, A. S.; Nordlander, P.; Halas, N. J. Near-Field Mediated Plexcitonic Coupling and Giant Rabi Splitting in Individual Metallic Dimers. *Nano Lett.* **2013**, *13*, 3281−3286.
(17) Ni, W. H.; Ambjornsson, T.; Apell, S. P.; Chen, H. J.; Wang, J. F. Observing Plasmonic-Molecular Resonance Coupling on Single Gold Nanorods. *Nano Lett.* **2010**, *10*, 77−84.
(18) Fofang, N. T.; Park, T. H.; Neumann, O.; Mirin, N. A.; Nordlander, P.; Halas, N. J. Plexcitonic Nanoparticles: Plasmon-Exciton Coupling in Nanoshell-J-Aggregate Complexes. *Nano Lett.* **2008**, *8*, 3481−3487.
(19) Wurtz, G. A.; Evans, P. R.; Hendren, W.; Atkinson, R.; Dickson, W.; Pollard, R. J.; Zayats, A. V.; Harrison, W.; Bower, C. Molecular Plasmonics with Tunable Exciton−Plasmon Coupling Strength in J-Aggregate Hybridized Au Nanorod Assemblies. *Nano Lett.* **2007**, *7*, 1297−1303.
(20) Bellessa, J.; Bonnand, C.; Plenet, J. C.; Mugnier, J. Strong Coupling between Surface Plasmons and Excitons in an Organic Semiconductor. *Phys. Rev. Lett.* **2004**, *93*, 036404.
(21) Wiederrecht, G. P.; Wurtz, G. A.; Hranisavljevic, J. Coherent Coupling of Molecular Excitons to Electronic Polarizations of Noble Metal Nanoparticles. *Nano Lett.* **2004**, *4*, 2121−2125.
(22) Yoshie, T.; Scherer, A.; Hendrickson, J.; Khitrova, G.; Gibbs, H. M.; Rupper, G.; Ell, C.; Shchekin, O. B.; Deppe, D. G. Vacuum Rabi Splitting with a Single Quantum Dot in a Photonic Crystal Nanocavity. *Nature* **2004**, *432*, 200−203.
(23) Ota, Y.; Shirane, M.; Nomura, M.; Kumagai, N.; Ishida, S.; Iwamoto, S.; Yorozu, S.; Arakawa, Y. Vacuum Rabi Splitting with a Single Quantum Dot Embedded in a H1 Photonic Crystal Nanocavity. *Appl. Phys. Lett.* **2009**, *94*, 033102.
(24) Glass, A. M.; Liao, P. F.; Bergman, J. G.; Olson, D. H. Interaction of Metal Particles with Adsorbed Dye Molecules: Absorption and Luminescence. *Opt. Lett.* **1980**, *5*, 368−370.
(25) Novotny, L.; Hecht, B. *Principles of Nano-Optics*; Cambridge University Press: Cambridge, U.K., 2006.
(26) Neogi, A.; Lee, C. W.; Everitt, H. O.; Kuroda, T.; Tackeuchi, A.; Yablonovitch, E. Enhancement of Spontaneous Recombination Rate in a Quantum Well by Resonant Surface Plasmon Coupling. *Phys. Rev. B: Condens. Matter Mater. Phys.* **2002**, *66*, 153305.
(27) Gryczynski, I.; Malicka, J.; Gryczynski, Z.; Lakowicz, J. R. Surface Plasmon-Coupled Emission with Gold Films. *J. Phys. Chem. B* **2004**, *108*, 12568−12574.
(28) Matveeva, E. G.; Gryczynski, Z.; Malicka, J.; Lukomska, J.; Makowiec, S.; Berndt, K. W.; Lakowicz, J. R.; Gryczynski, I. Directional Surface Plasmon-Coupled Emission: Application for an Immunoassay in Whole Blood. *Anal. Biochem.* **2005**, *344*, 161−167.
(29) Su, H. M.; Zhong, Y. C.; Ming, T.; Wang, J. F.; Wong, K. S. Extraordinary Surface Plasmon Coupled Emission Using Core/Shell Gold Nanorods. *J. Phys. Chem. C* **2012**, *116*, 9259−9264.
(30) Morton, S. M.; Jensen, L. Understanding the Molecule-Surface Chemical Coupling in SERS. *J. Am. Chem. Soc.* **2009**, *131*, 4090−4098.
(31) Lombardi, J. R.; Birke, R. L. A Unified Approach to Surface-Enhanced Raman Spectroscopy. *J. Phys. Chem. C* **2008**, *112*, 5605−5617.
(32) Tesema, T. E.; Kafle, B.; Habteyes, T. G. Plasmon-Driven Reaction Mechanisms: Hot Electron Transfer Versus Plasmon-Pumped Adsorbate Excitation. *J. Phys. Chem. C* **2019**, *123*, 8469−8483.
(33) Le Ru, E. C.; Meyer, S. A.; Artur, C.; Etchegoin, P. G.; Grand, J.; Lang, P.; Maurel, F. Experimental Demonstration of Surface Selection Rules for SERS on Flat Metallic Surfaces. *Chem. Commun.* **2011**, *47*, 3903−3905.
(34) Zhou, L.; Johnson, R.; Habteyes, T.; Guo, H. Adsorption of Methylene Blue and Its N-Demethylated Derivatives on the (111) Face of Coinage Metals: The Importance of Dispersion Interactions. *J. Chem. Phys.* **2017**, *146*, 164701.
(35) Moskovits, M. Surface-Enhanced Spectroscopy. *Rev. Mod. Phys.* **1985**, *57*, 783−826.
(36) Tesema, T. E.; Kafle, B.; Tadesse, M. G.; Habteyes, T. G. Plasmon-Enhanced Resonant Excitation and Demethylation of Methylene Blue. *J. Phys. Chem. C* **2017**, *121*, 7421−7428.
(37) Norrman, S.; Andersson, T.; Granqvist, C. G.; Hunderi, O. Optical-Properties of Discontinuous Gold-Films. *Phys. Rev. B: Condens. Matter Mater. Phys.* **1978**, *18*, 674−695.
(38) Luk'yanchuk, B.; Zheludev, N. I.; Maier, S. A.; Halas, N. J.; Nordlander, P.; Giessen, H.; Chong, C. T. The Fano Resonance in Plasmonic Nanostructures and Metamaterials. *Nat. Mater.* **2010**, *9*, 707−715.
(39) Habteyes, T. G.; Dhuey, S.; Cabrini, S.; Schuck, P. J.; Leone, S. R. Theta-Shaped Plasmonic Nanostructures: Bringing "Dark" Multipole Plasmon Resonances into Action Via Conductive Coupling. *Nano Lett.* **2011**, *11*, 1819−1825.
(40) Wang, S.; Boussaad, S.; Tao, N. J. Surface Plasmon Resonance Enhanced Optical Absorption Spectroscopy for Studying Molecular Adsorbates. *Rev. Sci. Instrum.* **2001**, *72*, 3055−3060.
(41) Darby, B. L.; Auguie, B.; Meyer, M.; Pantoja, A. E.; Le Ru, E. C. Modified Optical Absorption of Molecules on Metallic Nanoparticles at Sub-Monolayer Coverage. *Nat. Photonics* **2016**, *10*, 40.
(42) Zhong, X.; Rodrigo, S. G.; Zhang, L.; Samorì, P.; Genet, C.; Martín-Moreno, L.; Hutchison, J. A.; Ebbesen, T. W. Waveguide and Plasmonic Absorption-Induced Transparency. *ACS Nano* **2016**, *10*, 4570−4578.
(43) Hutchison, J. A.; O'Carroll, D. M.; Schwartz, T.; Genet, C.; Ebbesen, T. W. Absorption-Induced Transparency. *Angew. Chem., Int. Ed.* **2011**, *50*, 2085−2089.
(44) Naujok, R. R.; Duevel, R. V.; Corn, R. M. Fluorescence and Fourier-Transform Surface-Enhanced Raman-Scattering Measurements of Methylene-Blue Adsorbed onto a Sulfur-Modified Gold Electrode. *Langmuir* **1993**, *9*, 1771−1774.
(45) Foerster, B.; Spata, V. A.; Carter, E. A.; Sonnichsen, C.; Link, S. Plasmon Damping Depends on the Chemical Nature of the Nanoparticle Interface. *Sci. Adv.* **2019**, *5*, No. eaav0704.
(46) Kreibig, U. Interface-Induced Dephasing of Mie Plasmon Polaritons. *Appl. Phys. B: Lasers Opt.* **2008**, *93*, 79−89.
(47) Habteyes, T. G.; Dhuey, S.; Wood, E.; Gargas, D.; Cabrini, S.; Schuck, P. J.; Alivisatos, A. P.; Leone, S. R. Metallic Adhesion Layer Induced Plasmon Damping and Molecular Linker as a Nondamping Alternative. *ACS Nano* **2012**, *6*, 5702−5709.
(48) Tesema, T. E.; Annesley, C.; Habteyes, T. G. Plasmon-Enhanced Autocatalytic N-Demethylation. *J. Phys. Chem. C* **2018**, *122*, 19831−19841.
(49) McFarland, A. D.; Van Duyne, R. P. Single Silver Nanoparticles as Real-Time Optical Sensors with Zeptomole Sensitivity. *Nano Lett.* **2003**, *3*, 1057−1062.
(50) Zhao, J.; Jensen, L.; Sung, J. H.; Zou, S. L.; Schatz, G. C.; Van Duyne, R. P. Interaction of Plasmon and Molecular Resonances for Rhodamine 6G Adsorbed on Silver Nanoparticles. *J. Am. Chem. Soc.* **2007**, *129*, 7647−7656.
(51) Liu, M. Z.; Lee, T. W.; Gray, S. K.; Guyot-Sionnest, P.; Pelton, M. Excitation of Dark Plasmons in Metal Nanoparticles by a Localized Emitter. *Phys. Rev. Lett.* **2009**, *102*, 107401.
(52) Artuso, R. D.; Bryant, G. W.; Garcia-Etxarri, A.; Aizpurua, J. Using Local Fields to Tailor Hybrid Quantum-Dot/Metal Nanoparticle Systems. *Phys. Rev. B: Condens. Matter Mater. Phys.* **2011**, *83*, 235406.
(53) Kajetan Schmidt, M.; Mackowski, S.; Aizpurua, J. Control of Single Emitter Radiation by Polarization- and Position-Dependent Activation of Dark Antenna Modes. *Opt. Lett.* **2012**, *37*, 1017−1019.

https://dx.doi.org/10.1021/acs.jpclett.0c00734
J. Phys. Chem. Lett. 2020, 11, 3507−3514